Development of robust fractional-order reset control

Chen, Linda; Saikumar, Niranjan; Hossein Nia Kani, Hassan

DOI
10.1109/TCST.2019.2913534

Publication date
2019

Document Version
Accepted author manuscript

Published in
IEEE Transactions on Control Systems Technology

Development of Robust Fractional-Order Reset Control

Linda Chen, Niranjan Saikumar, and S. Hassan HosseinNia, *Senior Member, IEEE*

***Abstract*— In this paper, a framework for the combination of robust fractional-order CRONE control with nonlinear reset is given for both first and second generation CRONE control. General design rules are derived and presented for these CRONE reset controllers. Within this framework, fractional-order control allows for better tuning of the open-loop responses on the one hand. On the other hand, reset control enables a reduction in phase lag and a corresponding increase in phase margin compared to linear control for similar open-loop gain profile. Hence, the combination of the two control methods can provide well-tuned open-loop responses that can overcome the fundamental linear control limitation of Bode's gain-phase relationship. Moreover, as established loop-shaping concepts are used in the controller design, CRONE reset can be highly compatible with the industry. The designed CRONE reset controllers are validated on a one degree-of-freedom Lorentz-actuated precision positioning stage. On this setup, CRONE reset control is shown to provide better tracking performance compared to linear CRONE control, which is in agreement with the predicted performance improvement.**

***Index Terms*— CRONE, CRONE reset control, fractional-order control, fractional-order reset control, loop shaping, mechatronics, nonlinear control, precision motion control, reset control, robust control.**

I. Introduction

MOTION control in (sub)nanometre precision positioning remains a present-day challenge in the high-tech industry. Advances in semiconductor manufacturing, production of microscale and nanoscale electronic devices (MEMS and NEMS), and imaging of nanostructures are among the applications that have increased demand for high degree of precision positioning systems. Conventional and popular proportional—integral—differential (PID) controllers and even other linear controllers find it increasingly difficult to satisfy the demands in presence of uncertainties, which become more prominent when moving to smaller scales and higher bandwidths. In linear control, fundamental relations as the Bode's gain-phase relation and the waterbed effect [1] inevitably establish tradeoffs between system performance in terms of reference tracking, noise attenuation and disturbance rejection, and robustness. This makes precision positioning control an interesting problem from both system design and control point of view, considered, for instance, in [2] and [3].

In Commande Robuste d'Ordre Nonentier (CRONE—translates to noninteger order robust control) control [4] additional flexibility in the tradeoff between robustness and performance is obtained using fractional operators. Although fundamental relations of linear control still apply, the fractional operators allow for better and easier tuning of required stability margins and open-loop shape. To overcome Bode's gain-phase relation and provide greater relief to the robustness-performance trade off, nonlinear reset control is considered.

Nonlinear reset control has been the focus of many researchers in past and present years, starting from the first work of Clegg [5]. In this work, a reset integrator [also known as Clegg integrator (CI)] was introduced: an integrator that is reset when its error input equals zero. Using describing function analysis [6], it is seen that the reset integrator has a phase lag of only 38°, hence providing 52° phase lead with respect to a linear integrator for the same −20 dB/decade gain slope. Recognizing the potential of this profitable gain-phase characteristic, several works prove the improved performance using reset control, such as [7] and [8]. Alternative resetting laws for improved robustness and/or performance have also been proposed. These include partial reset (nonzero after-reset state value), variable reset [9], both constant and variable reset band in [10] and [11], respectively, and (variable [12]) reset percentages in the PI+CI compensator approach (PI controller with a reset integrator), for which a control design framework has been developed in [13]. Other resetting conditions include resetting at fixed time instants rather than fixed state values [14], quadratic resetting conditions [15] and conditions obtained in an optimization problem [16].

For these reset approaches, stability theorems have been developed. Generally, the works concerning stability proofs can be divided into Lyapunov-based and passivity-based proofs [17]. In the former, the H_β-condition [18] is one of the conditions with which one can prove stability for reset systems with stable linear base. In a recent work, sufficient stability conditions based on the measured frequency responses are given [15], which aims to eliminate the need for solving linear matrix inequalities (LMIs) present in most of the previous stability conditions and, thus, making reset controllers more accessible to control engineers in industry. As a result of the existing research, many applications of reset control exists. Examples include applications in process control [19], [20], positioning systems [9], [21], and hard-drive disks [22], [23].

Manuscript received December 20, 2018; accepted April 17, 2019. Manuscript received in final form April 23, 2019. Recommended by Associate Editor R. Tóth. *(Corresponding author: S. Hassan HosseinNia.)*

L. Chen was with the Delft Center for Systems and Control, Delft University of Technology, 2628 Delft, The Netherlands. She is now with Hoogewerf Engineering BV, 1948 RL Beverwijk, The Netherlands (e-mail: lindachen93@gmail.com).

N. Saikumar and S. H. HosseinNia are with the Department of Precision and Microsystems Engineering, Delft University of Technology, 2628 Delft, The Netherlands (e-mail: n.saikumar@tudelft.nl; s.h.hosseinniakani@tudelft.nl).

Color versions of one or more of the figures in this paper are available online at http://ieeexplore.ieee.org.

Digital Object Identifier 10.1109/TCST.2019.2913534

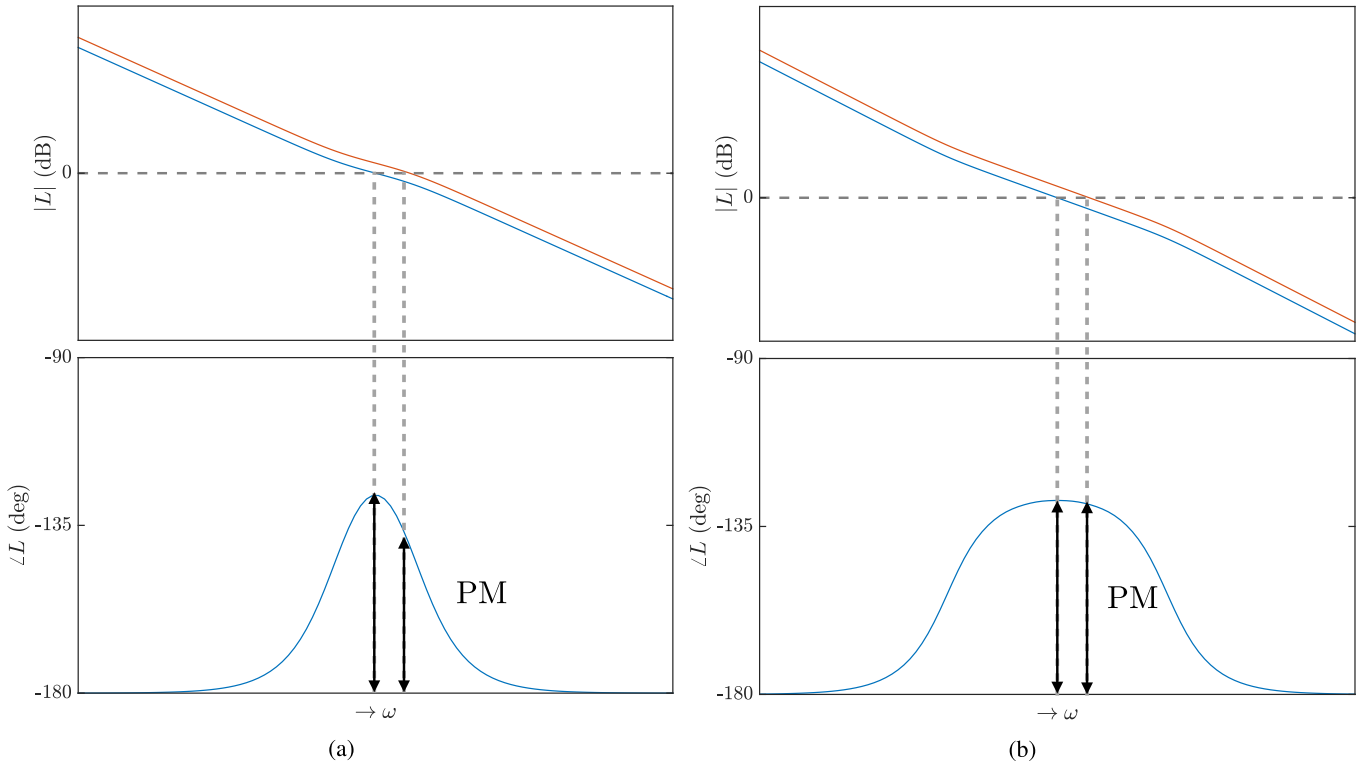

Fig. 1. (a) Typical open-loop response with conventional linear controllers. Under gain variations, the phase margin (PM) fluctuates. (b) After achieving constant phase in the frequency range around bandwidth, the phase margin is close to constant.

Still, reset control synthesis remains an actively researched topic.

In the works of [24] and [25], the framework for fractional-order reset has already been mathematically founded. Several works in this field include generalization of the CI, PI+CI and first-order reset element (FORE) to CI$^\alpha$ [25], PI$^\alpha$+CI$^\alpha$ [25], and GFrORE [26], respectively. In [27], a fractional-order reset system with an iterative learning algorithm was proposed to increase robustness in the presence of model uncertainties and avoid limit cycles simultaneously.

Although fractional-order reset control exists in the literature, reset applied to CRONE control specifically has not yet been done. The motivation for this paper arises from the fact that a robust design methodology already exists with CRONE. However, as noted earlier, CRONE controllers are linear and hence suffer from fundamental limitations. This paper aims to extend this design methodology to include reset actions to obtain further relief in the robustness-performance tradeoff and provide new design rules for robust fractional-order reset control. The preliminary work with this regard has been presented in [28] with reset introduced into the first generation CRONE controllers. However, the second-generation CRONE that can provide robust performance even in the case of nonasymptotic phase behavior for the system in the region of bandwidth is of greater interest to the precision control community. The ideas for the first-generation CRONE are provided and then extended for the second generation in this paper. In addition, apart from the analysis of results obtained from the second generation CRONE reset, the performance in terms of disturbance rejection for both generations has also been addressed in this paper.

This paper is structured as follows. Section II concerns fundamentals of CRONE control and reset control. Then follows the formulation of CRONE reset control and design rules in Section III. The practical application of designed CRONE reset controllers is given in Section IV, followed by a discussion of experimental results in Section V. Finally, conclusions are provided in Section VI.

II. Preliminaries

A. Robust CRONE Control

The CRONE control framework provides a methodology for robust fractional-order control design. Robustness is achieved by the creation of constant phase around open-loop bandwidth. This can be seen in Fig. 1. Under system gain deviations, robustness of the system is ensured as phase margin remains equal. Three generations of CRONE control have been formalized in [4]. Only the first two generations of CRONE are considered in this work: CRONE-1 and CRONE-2. CRONE-1 can be used for plants with asymptotic phase behavior around the required bandwidth. CRONE-2 can be used for plants without this asymptotic phase behavior. Both generations of CRONE provide robustness against gain deviation. CRONE-3 control uses complex fractional order, which is not practically implementable and thus not taken further into account.

1) First Generation CRONE: A first generation CRONE controller, also referred to as CRONE-1, has a similar transfer function to an integer-order series PID controller

$$C_F(s) = C_0 \left(1 + \frac{\omega_I}{s}\right)^{n_I} \left(\frac{1 + \frac{s}{\omega_b}}{1 + \frac{s}{\omega_h}}\right)^{\nu} \frac{1}{\left(1 + \frac{s}{\omega_F}\right)^{n_F}} \quad (1)$$

with ω_I and ω_F being the integrator- and low-pass filter corner frequencies, ω_b and ω_h the corner frequencies of the band-limited derivative action, $\nu \in \mathbb{R} \cap [0, 1]$ the fractional order of the derivative action, and $n_I, n_F \in \mathbb{N}$ being the order of the integrator and low-pass filter, respectively. The difference between a series integer-order PID controller and a first generation CRONE controller is that the order ν is fractional instead of an integer, making first generation CRONE "a fractional PID controller." The flat phase behavior illustrated in Fig. 1(b) is created by choosing a wider frequency range in which the derivative action is active (compared to PID control) and by decreasing the order ν to a fractional value.

The fractional order ν can be calculated from

$$\nu = \frac{-\pi + M_\Phi - \arg G(j\omega_{cg}) + n_F \arctan \frac{\omega_{cg}}{\omega_F} + n_I \left(\frac{\pi}{2} - \arctan \frac{\omega_{cg}}{\omega_I}\right)}{\arctan \frac{\omega_{cg}}{\omega_b} - \arctan \frac{\omega_{cg}}{\omega_h}} \quad (2)$$

where $G(j\omega)$ is the plant frequency response and M_Φ is the required phase margin. The gain C_0 is chosen such that the loop gain at frequency ω_{cg} is equal to 1.

2) Second Generation CRONE: In the second generation CRONE, which is alternatively addressed as CRONE-2, the desired open loop is first designed. The resulting controller is comprised of this desired open loop in series with the plant inverse.

Desired open-loop $\beta_0(s)$ is given as

$$\beta_0(s) = C_0 \left(1 + \frac{\omega_I}{s}\right)^{n_I} \left(\frac{1 + \frac{s}{\omega_b}}{1 + \frac{s}{\omega_h}}\right)^{-\nu} \frac{1}{\left(1 + \frac{s}{\omega_F}\right)^{n_F}} \quad (3)$$

where the order $\nu \in \mathbb{R} \cap [1, 2]$ is again fractional and given by

$$\nu = \frac{-\pi + M_\Phi + n_F \arctan \frac{\omega_{cg}}{\omega_F} + n_I \left(\frac{\pi}{2} - \arctan \frac{\omega_{cg}}{\omega_I}\right)}{\arctan \frac{\omega_{cg}}{\omega_h} - \arctan \frac{\omega_{cg}}{\omega_b}}. \quad (4)$$

The second generation CRONE controller finally has the following structure

$$C_S(s) = G_0^{-1}(s)\beta_0(s) \quad (5)$$

in which $G_0(s)$ is the nominal plant.

In both CRONE-1 and CRONE-2, the resulting fractional-order derivative is approximated in the required frequency range using CRONE approximation [4]. The resulting higher order integer-order transfer function approximates the required fractional-order derivative's frequency behavior.

B. Reset Control

A general reset system can be described using the following impulsive differential equations, according to the formalism in [18]:

$$\Sigma_R := \begin{cases} \dot{x}_R(t) = A_R x_R(t) + B_R e(t), & \text{if } e(t) \neq 0 \\ x_R(t^+) = A_\rho x_R(t), & \text{if } e(t) = 0 \\ u(t) = C_R x_R(t) + D_R e(t) \end{cases} \quad (6)$$

where matrices A_R, B_R, C_R, and D_R are the base linear state-space matrices of the reset controller, $e(t)$ is the error between output and reference, $u(t)$ is the control input signal, $x_R(t)$ are the states with $x_R = [x_r^T \quad x_{\text{nr}}^T]^T$ where x_r are the n_r number of states being reset and x_{nr} are the n_{nr} states not being reset with $n_r + n_{nr} = n_R$ (total number of states of feedback controller), and A_ρ is the reset matrix. A_ρ is designed as a diagonal matrix with the elements corresponding to states x_{nr} equal to one.

When the frequency response of a reset system is approximated using describing function analysis, it is seen that phase lag is significantly reduced by the nonlinearity.

1) Describing Function Analysis: The general describing function of a reset system as defined in [29] is given by

$$G_{\text{DF}}(j\omega) = C_R(j\omega I - A_R)^{-1} B_R(I + j\Theta_D(\omega)) + D_R \quad (7)$$

where $\Theta_D(\omega)$ is defined as

$$\Theta_D(\omega) = -\frac{2\omega^2}{\pi} \Delta(\omega)[\Gamma_D(\omega) - \Lambda^{-1}(\omega)]. \quad (8)$$

The definitions of the set of equations used are given in the following:

$$\begin{cases} \Lambda(\omega) = \omega^2 I + A_R^2 \\ \Delta(\omega) = I + e^{\frac{\pi}{\omega} A_R} \\ \Delta_D(\omega) = I + A_\rho e^{\frac{\pi}{\omega} A_R} \\ \Gamma_D(\omega) = \Delta_D^{-1}(\omega) A_\rho \Delta(\omega) \Lambda^{-1}(\omega). \end{cases}$$

2) General Stability Analysis: The reset system given in (6) can be represented in closed loop as

$$\begin{cases} \dot{x}(t) = A_{cl} x(t) + B_{cl} w(t), & \text{if } x(t) \notin \mathcal{M}(t) \\ x(t^+) = A_{\rho_{cl}} x(t), & \text{if } x(t) \in \mathcal{M}(t) \\ u(t) = C_{cl} x(t) + d(t) \\ e(t) = w(t) - C_{cl} x(t) \end{cases} \quad (9)$$

where $x = [x_p^T \quad x_R^T]^T$

$$A_{cl} = \begin{bmatrix} A_p & B_p C_r \\ -B_R C_p & A_R \end{bmatrix}, \quad B_{cl} = \begin{bmatrix} 0 \\ B_R \end{bmatrix}$$

$$A_{\rho_{cl}} = \begin{bmatrix} I_{n_p} & 0 \\ 0 & A_\rho \end{bmatrix}, \quad C_{cl} = \begin{bmatrix} C_p & 0 \end{bmatrix}$$

with A_p, B_p, and C_p being the state-space matrices of the plant to be controlled with n_p number of states and reset surface $\mathcal{M}(t)$ is given as

$$\mathcal{M}(t) = \left\{ \xi \in \mathbb{R}^{n_p + n_r} : e(t) = 0, (I - A_R)\xi \neq 0 \right\}.$$

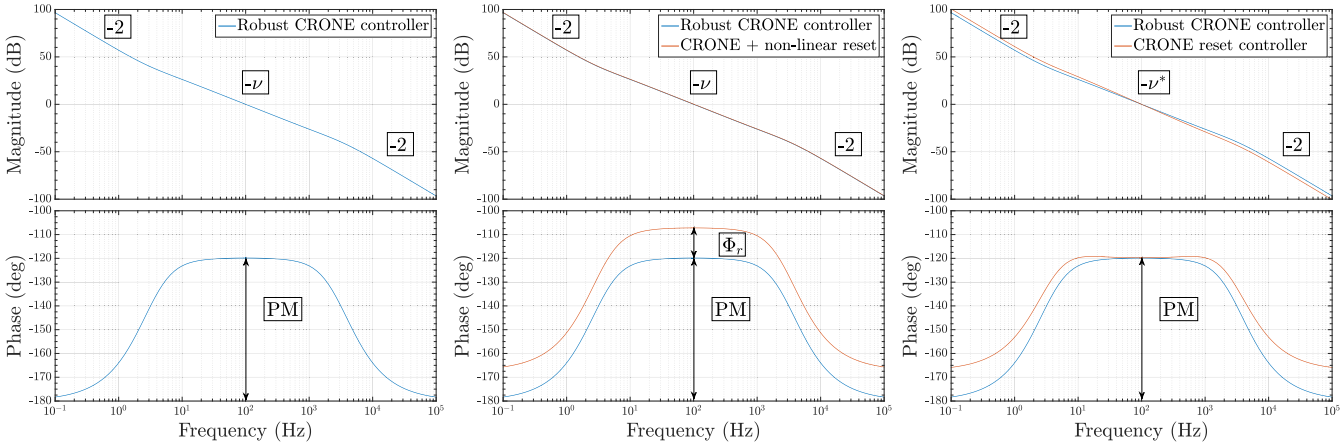

Fig. 2. Frequency-domain open-loop responses showing CRONE reset control concept. Open-loop with indication of open-loop slopes for (a) step 1: robust CRONE controller, (b) step 2: additional nonlinear reset adds phase Φ_r, and (c) step 3: improved open-loop shape with new fractional slope $\nu^* > \nu$.

Theorem 1 [30]: Let $V : \mathbb{R}^n \to \mathbb{R}$ be a continuously differentiable, positive definite, radially unbounded function such that

$$\dot{V}(x) := \left(\frac{\partial V}{\partial x}\right)^T A_{cl}x < 0, \quad \text{if } x \neq 0 \tag{10}$$

$$\Delta V(x) := V(A_{\rho_{cl}}x) - V(x) \leq 0, \quad \text{if } x \in \mathcal{M}. \tag{11}$$

Then, the equilibrium point $x = 0$ is globally uniformly asymptotically stable.

From this condition, Beker *et al.* [30] obtained the following theorem for proving quadratic stability:

Theorem 2 [30]: The reset control system (9) is said to satisfy the H_β condition if there exists a constant $\beta \in \mathbb{R}^{n_r}$ and positive-definite $P_\rho \in \mathbb{R}^{n_r \times n_r}$, such that

$$H_\beta(s) = \begin{bmatrix}\beta C_p & O_{n_r \times n_{nr}} & P_\rho\end{bmatrix}(sI - A_{cl})^{-1}\begin{bmatrix}O_{n_p \times n_r} \\ O_{n_{nr} \times n_r} \\ I_{n_r}\end{bmatrix} \tag{12}$$

is strictly positive real. The reset control system in (6) is quadratically stable if and only if it satisfies the H_β condition.

This H_β condition has been used in this paper for stability analysis. However, this is not the only stability theorem for reset systems present in the literature. For example, Nešić *et al.* [31] provides the conditions for L_p stability for arbitrary $p \in [1, \infty)$. Since the focus of this paper is not on developing stability theorems, this is not discussed in greater detail.

III. Robust CRONE Reset Control

CRONE control by itself is fundamentally limited as a linear controller. Thus, being a robust controller, the system may underperform in terms of tracking, disturbance rejection, and noise attenuation as a result of fundamental tradeoffs in linear control. It is, in this scenario, that nonlinear reset can provide relief. The novel combination of CRONE and reset control will be addressed as CRONE reset control. The CRONE reset control concept can be broken down into three steps as follows.

1) Design of robust CRONE controller.
2) Addition of phase around bandwidth with nonlinear reset.
3) Retuning of open-loop slope around bandwidth to improve open-loop shape for same phase margin.

The first step results in a linear controller that is robust and, hence, suffers in tracking and noise attenuation. The introduction of reset and the subsequent retuning results in robustness being retained with the improvement in other performance characteristics. Above procedure is summarized in the open-loop responses depicted in Fig. 2. In the final step as depicted in Fig. 2(c), it can be seen that open-loop gain has improved at both low and high frequencies (for better tracking and improved attenuation of noise, respectively) with respect to the linear CRONE case in Fig. 2(a).

CRONE reset control design requires computation of a new slope around bandwidth ν^*. This value differs, depending on the amount of phase added by resetting action, and thus varies for different reset strategies. In this section, first, reset strategies are formulated, a CRONE reset control structure is established and the new design rules are given for the calculation of slope ν^* for a selection of reset strategies for both CRONE-1 reset and CRONE-2 reset. Finally, the general stability analysis, as introduced in Section II-B2, is adapted for the developed CRONE reset control framework.

A. Reset Strategies

We define reset strategy as a unique combination of choices for: base controller, part of controller transfer function to be reset, the order of the part to be reset, and the selection of reset approaches.

In the following, the construction of a reset strategy is illustrated for CRONE-1 reset as an example

$$C_F(s) = \Sigma_r \Sigma_{nr} \tag{13}$$

in which Σ_{nr} is the linear part and Σ_r is the reset part of the transfer function as given in (1). The reset part could be one of the following.

1) Integrator part (ω_I/s).
2) Lead/lag part

$$\left(\frac{1+\frac{s}{\omega_b}}{1+\frac{s}{\omega_h}},\ \text{lead}:\omega_b<\omega_h,\ \text{lag}:\omega_b>\omega_h\right).$$

3) First-order filter part

$$\left(\frac{1}{1+\frac{s}{\omega_h}}\ or\ \frac{1}{1+\frac{s}{\omega_l}}\right).$$

These reset elements can be of first order or higher. However, in this paper, we focus on the FOREs only.

With the second of three choices listed above, the lead and lag filters are assessed in two different ways. In the case of both lag and lead filters, resetting can be performed either only on the pole or on the pole-zero combination and results in unique frequency response. This is as shown in Table. I. In the case where only the pole is reset as shown in the top row of Table I, the zero part is made proper by combining with the low-pass filter part of the designed CRONE controller.

Comparing the amount of additional phase lag reduction seen, resetting of lag part is more favorable than resetting of lead part. Thus, the remaining of this paper will focus on the following.

1) Integrator part (ω_i/s).
2) Lag part.
3) First-order filter part ($1/(1+(s/\omega_b))$).

As in the literature, different approaches can be taken to reset [18].

1) Partial reset—where the state is not reset to zero resulting in the corresponding element of A_ρ having a nonzero value.
2) Reset percentage—which uses the PI+CI compensator approach of having a PI loop in parallel with CI. Both loops have a weight assigned to them with the combined weight equalling one.
3) Variable reset—where the nonzero value of partial reset and/or the weights of reset percentage are not fixed and can vary during operation.
4) Reset band—where the reset is carried out when the error signal enters a band instead of zero-crossing.

The describing function analysis in the case of variable reset and reset band is not straightforward and the equations provided in Section II-B1 are not valid making design and analysis difficult. Also, these approaches are not robust and, hence, are not considered. Partial reset and reset percentage both provide ways to control the level of reset and hence nonlinearity and phase lag reduction achieved.

B. Control Structure

The chosen reset approaches of partial reset and reset percentage constitute a CRONE reset controller with two degrees of freedom in tuning nonlinearity in the system. The general state-space representation of the CRONE reset control system Σ_R that consists of the reset part Σ_r and nonreset part

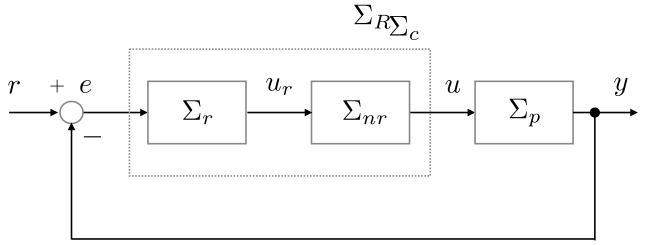

Fig. 3. Control structure of the CRONE reset controller Σ_R, which contains a linear part Σ_{nr} and a nonlinear reset part Σ_r. Σ_p is the plant being controlled.

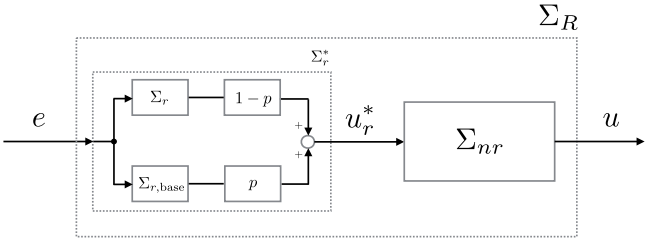

Fig. 4. Structure of the CRONE reset controller Σ_R with two-degree-of-freedom nonlinearity tuning, which contains a linear part Σ_{nr} and a nonlinear reset part Σ_r with $A_\rho=\gamma I$. $\Sigma_{r,\text{base}}$ is the base linear system of Σ_r.

Σ_{nr} is constituted as follows:

$$\Sigma_r := \begin{cases} \dot{x}_r(t) = A_r x_r(t) + B_r e(t), & \text{if } e(t)\neq 0 \\ x_r(t^+) = \bar{A_\rho} x_r(t), & \text{if } e(t)=0 \\ u_r(t) = C_r x_r(t) + D_r e(t) \end{cases} \tag{14}$$

$$\Sigma_{nr} := \begin{cases} \dot{x}_{nr}(t) = A_{nr} x_{nr}(t) + B_{nr} u_r(t) \\ u_{nr}(t) = C_{nr} x_{nr}(t) + D_{nr} u_r(t) \end{cases} \tag{15}$$

$$\Sigma_R := \begin{cases} \dot{x}_R(t) = A_R x_R(t) + B_R e(t), & \text{if } e(t)\neq 0 \\ x_R(t^+) = A_\rho x_R(t), & \text{if } e(t)=0 \\ u(t) = C_R x_R(t) + D_R e(t) \end{cases} \tag{16}$$

where $e(t)$ is the error signal, $u_r(t)$ is the output of Σ_r which is, in-turn, input to the nonreset part, $x_r(t)$, $x_{\text{nr}}(t)$, and $x_R(t)=\begin{bmatrix}x_r^T & x_{nr}^T\end{bmatrix}^T$ are the reset-controller states, nonreset controller states, and CRONE reset controller states, respectively, and A_ρ, $\bar{A}_\rho$ are the reset matrices. Matrices A_R, B_R, C_R, and D_R are the base linear state-space matrices of the reset system, defined as

$$A_R = \begin{bmatrix} A_r & O \\ B_{nr}C_r & A_{nr} \end{bmatrix} \tag{17}$$

$$B_R = \begin{bmatrix} B_r \\ B_{nr}D_r \end{bmatrix} \tag{18}$$

$$C_R = \begin{bmatrix} D_{nr}C_r & C_{nr} \end{bmatrix} \tag{19}$$

$$D_R = D_{nr}D_r \tag{20}$$

and reset matrix A_ρ is defined as

$$A_\rho = \text{diag}(\bar{A_\rho}, I_{n_{nr}}). \tag{21}$$

The structure of this controller Σ_R is shown in Fig. 3.

Slight alterations are made to the system definitions from (14) to (16) to obtain two degrees of freedom in tuning nonlinearity within the system. The first chosen reset approach of partial reset establishes the first degree of freedom; reset

TABLE I

DESCRIBING FUNCTION FOR RESETTING DIFFERENT PARTS OF A LEAD AND A LAG FILTER. LAG RESET PROVIDES MORE PHASE AT BANDWIDTH THAN LEAD RESET. RESET OF THE FIRST-ORDER FILTER WITH LOWER CORNER FREQUENCY ω_b PROVIDES MORE PHASE AT BANDWIDTH THAN THE SAME FILTER WITH HIGHER CORNER FREQUENCY ω_l

Reset part	lead filter $\left(\frac{1+\frac{s}{\omega_l}}{1+\frac{s}{\omega_h}}\right)$	lag filter $\left(\frac{1+\frac{s}{\omega_h}}{1+\frac{s}{\omega_l}}\right)$
first order filter reset	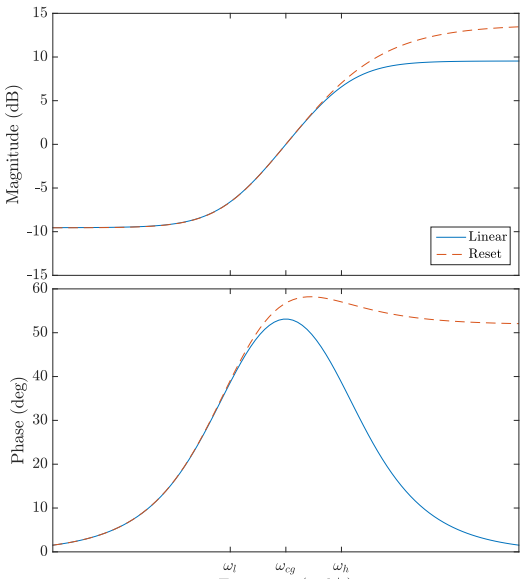 $\underbrace{(1+\frac{s}{\omega_l})}_{\Sigma_{nr}}\underbrace{\frac{1}{1+\frac{s}{\omega_h}}}_{\Sigma_r}$	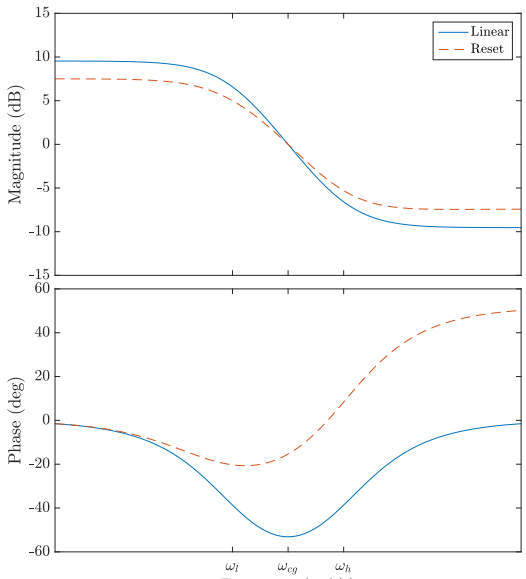 $\underbrace{(1+\frac{s}{\omega_h})}_{\Sigma_{nr}}\underbrace{\frac{1}{1+\frac{s}{\omega_l}}}_{\Sigma_r}$
lag/lead reset	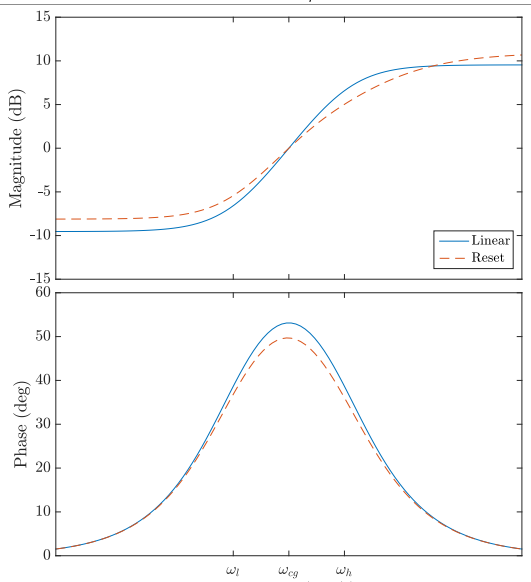 $\underbrace{\frac{1+\frac{s}{\omega_l}}{1+\frac{s}{\omega_h}}}_{\Sigma_r}$	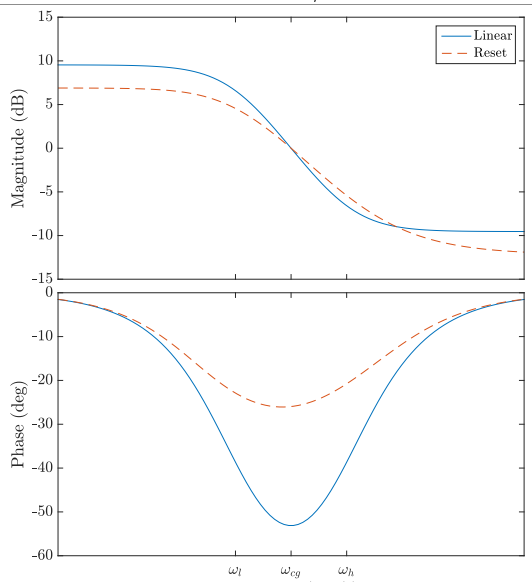 $\underbrace{\frac{1+\frac{s}{\omega_h}}{1+\frac{s}{\omega_l}}}_{\Sigma_r}$

matrix $\bar{A_\rho}$ is taken as

$$\bar{A_\rho} = \gamma\, I_{n_r} \tag{22}$$

where I_{n_r} is an identity matrix of size n_r with n_r being the number of reset states. With this reset matrix, the after-reset state value $x_r(t^+)$ is a fraction γ of the before-reset state value $x_r(t)$. When $\gamma = 0$ traditional reset occurs, whereas the system simplifies to a full linear system when $\gamma = 1$. The conditions for the open-loop stability of such a reset controller with nonzero resetting matrix are provided in [29].

The second chosen reset approach of reset percentage forms the second degree of freedom in tuning nonlinearity in the

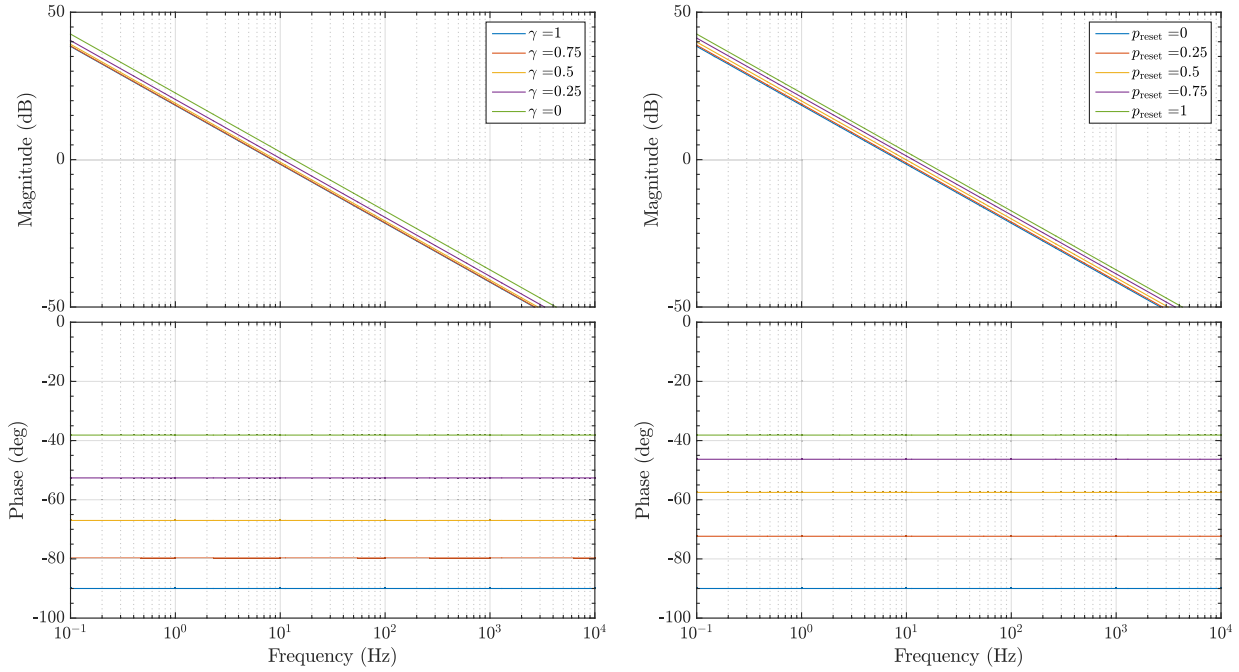

Fig. 5. Describing function of a reset integrator when tuning nonlinearity (a) for different values of γ with $p = 0$ and (b) for different values of p with $\gamma = 0$.

system. A convex combination between the reset part Σ_r and its linear base system $\Sigma_{r,\text{base}}$ is taken as shown in Fig. 4 in Σ_r^*. p is the percentage of linearity in the system. When $p = 0$, Σ_r^* is equivalent to Σ_r and when $p = 1$, the system becomes fully linear.

The describing function of both reset approaches applied to a reset integrator is shown in Fig. 5. It is evident that with both reset approaches, the nonlinearity in the system can be tuned and the amount of reset phase lead can be adjusted.

C. New Design Rules

As noted at the beginning of this section, the design of CRONE reset controller consists of three steps with the first step being the design of linear CRONE controller. This is followed by a selection of reset strategy involving choice over Σ_r and choice of control structure variables γ and p. With these choices, the application of reset results in reduction in phase lag compared to its linear counterpart. This reduction which can be seen as phase lead achieved through reset can be calculated using describing function analysis for both CRONE-1 reset and CRONE-2 reset control.

1) Derivation Reset Phase Lead: A linear combination is made between describing function of the reset system and its linear base equivalent to include the convex-combination structure with reset percentage p

$$G_{\text{DF}}^*(j\omega) = p(C(j\omega I - A)^{-1}B + D) + (1-p)(C(j\omega I - A)^{-1}B(I + j\Theta_D(\omega)) + D). \tag{23}$$

The additional phase at bandwidth is given by $\Phi_r(\omega_{cg})$, which is retrieved by filling in $\omega = \omega_{cg}$ in

$$\Phi_r(\omega) = \angle G_{\text{DF}}^*(j\omega) - \angle G(j\omega). \tag{24}$$

2) Reset Strategy-Dependent Phase Lead: The amount of phase lead achieved by resetting is different depending on the chosen reset strategy. The reset phase leads are directly derived from (23) and (24) and given in the following for different reset strategies.

a) CRONE integrator reset: The reset phase lead for an integrator reset is

$$\Phi_{r,\text{int}}(\gamma, p) = \arctan\left(\frac{4}{\pi}(1-p)\frac{1-\gamma}{1+\gamma}\right) \tag{25}$$

which is frequency independent.

b) CRONE lead/lag reset: As a base filter to define lead/lag reset strategy and finally acquire the controller representation in the form of (14)–(16), first consider following filter:

$$H_{\text{ll}}(s) = \frac{1+\frac{s}{a}}{1+\frac{s}{b}} \tag{26}$$

where a and b are the corner frequencies. For such first-order filters $\Theta_D(\omega)$, as in (8), is expressed as

$$\Theta_D(\omega, b, \gamma) = \frac{2}{\pi}\frac{1+e^{-\pi\frac{b}{\omega}}}{1+\left(\frac{b}{\omega}\right)^2}\frac{1-\gamma}{1+\gamma\, e^{-\pi\frac{b}{\omega}}}. \tag{27}$$

Then, the phase lead for $H_{\rm ll}(s)$ in (26) with partial reset γ and reset percentage p can be computed using (24) as

$$\Phi_{r,\rm ll}(\omega, a, b, \gamma, p) = \arctan\left(\frac{(1-p)\Theta_D(\omega, b, \gamma)\left(1-\frac{b}{a}\right)}{1+\left(\frac{\omega}{a}\right)^2+(1-p)\frac{\omega}{a}\Theta_D(\omega, b, \gamma)\left(1-\frac{b}{a}\right)}\right). \tag{28}$$

c) CRONE first-order filter reset: When, in (26), $a \to \infty$ $H_{ll}(s)$ simplifies to a first-order filter. Therefore, the phase lead of (28) becomes

$$\Phi_{r,\rm fof}(\omega, b, \gamma, p) = \arctan((1-p)\Theta_D(\omega, b, \gamma)). \tag{29}$$

Using the phase leads achieved with resetting in (25)–(29) for different reset strategies and applying (36) and (37), the reset strategies applied to CRONE-1 and CRONE-2 are illustrated in Sections III-C.3–III-C.4.

3) CRONE-1 Reset: Applying the new design rules to specific reset strategies for CRONE-1 results in the following.

a) CRONE-1 integrator reset:

$$C_{\rm int}(s) = \underbrace{\left(\frac{\omega_I}{s}\right)^{n_I-1} C_0\left(\frac{s}{\omega_I}+1\right)^{n_I}\left(\frac{1+\frac{s}{\omega_b}}{1+\frac{s}{\omega_h}}\right)^{\nu}\frac{1}{\left(1+\frac{s}{\omega_F}\right)^{n_F}}}_{\Sigma_{nr}}\underbrace{\frac{\omega_I}{s}}_{\Sigma_r} \tag{30}$$

and phase lead with integrator reset is given by (25).

b) CRONE-1 lag reset:

$$C_{\rm lag}(s) = \underbrace{\left(\frac{1+\frac{s}{\omega_b}}{1+\frac{s}{\omega_h}}\right)^{\nu+1} C_0\left(1+\frac{\omega_I}{s}\right)^{n_I}\frac{1}{\left(1+\frac{s}{\omega_F}\right)^{n_F}}}_{\Sigma_{nr}}\underbrace{\frac{1+\frac{s}{\omega_h}}{1+\frac{s}{\omega_b}}}_{\Sigma_r} \tag{31}$$

and phase lead with lag reset is given by (28) with $b = \omega_b$ and $a = \omega_h$.

In the case of CRONE-1, it should be noted that the linear CRONE-1 has a lead element since the structure of CRONE-1 is similar to that of PID. However, according to Table I, since resetting lag part results in more lag reduction, a lag element is introduced with a corresponding

c) CRONE-1 first-order filter reset:

$$C_{\rm fof}(s) = \underbrace{\frac{\left(1+\frac{s}{\omega_b}\right)^{\nu+1}}{(1+\frac{s}{\omega_h})^{\nu}} C_0\left(1+\frac{\omega_I}{s}\right)^{n_I}\frac{1}{\left(1+\frac{s}{\omega_F}\right)^{n_F}}}_{\Sigma_{nr}}\underbrace{\frac{1}{1+\frac{s}{\omega_b}}}_{\Sigma_r} \tag{32}$$

and phase lead with the first-order filter reset is given by (29) with $b = \omega_b$.

4) CRONE-2 Reset: Results for CRONE-2 reset are retrieved as the following.

a) CRONE-2 integrator reset:

$$\beta_{0,\rm int}(s) = \underbrace{\left(\frac{\omega_I}{s}\right)^{n_I-1} C_0\left(\frac{s}{\omega_I}+1\right)^{n_I}\left(\frac{1+\frac{s}{\omega_b}}{1+\frac{s}{\omega_h}}\right)^{-\nu}\frac{1}{\left(1+\frac{s}{\omega_F}\right)^{n_F}}}_{\Sigma_{nr}}\underbrace{\frac{\omega_I}{s}}_{\Sigma_r} \tag{33}$$

and phase lead with integrator reset is given by (25).

b) CRONE-2 lag reset:

$$\beta_{0,\rm lag}(s) = \underbrace{\left(\frac{1+\frac{s}{\omega_b}}{1+\frac{s}{\omega_h}}\right)^{-(\nu-1)} C_0\left(1+\frac{\omega_I}{s}\right)^{n_I}\frac{1}{\left(1+\frac{s}{\omega_F}\right)^{n_F}}}_{\Sigma_{nr}}\underbrace{\frac{1+\frac{s}{\omega_h}}{1+\frac{s}{\omega_b}}}_{\Sigma_r} \tag{34}$$

and phase lead with lag reset is given by (28) with $b = \omega_b$ and $a = \omega_h$.

c) CRONE-2 first-order filter reset:

$$\beta_{0,\rm fof}(s) = \underbrace{\frac{\left(1+\frac{s}{\omega_b}\right)^{-(\nu-1)}}{\left(1+\frac{s}{\omega_h}\right)^{-\nu}} C_0\left(1+\frac{\omega_I}{s}\right)^{n_I}\frac{1}{\left(1+\frac{s}{\omega_F}\right)^{n_F}}}_{\Sigma_{nr}}\underbrace{\frac{1}{1+\frac{s}{\omega_b}}}_{\Sigma_r} \tag{35}$$

and phase lead with the first-order filter reset is given by (29) with $b = \omega_b$.

Once the phase lead achieved through the application of reset is calculated for the chosen reset strategy and reset variables, new slope ν^* as a function of reset phase lead at bandwidth frequency $\Phi_r(\omega_{\rm cg})$ can be calculated as (36), shown at the bottom of this page, with $\nu^* \in [0, 1]$ for CRONE-1 and

$$\nu^* = \frac{-\pi + M_\Phi + n_F \arctan\frac{\omega_{cg}}{\omega_F} + n_I\left(\frac{\pi}{2} - \arctan\frac{\omega_{cg}}{\omega_I}\right) - \Phi_r(\omega_{cg})}{\arctan\frac{\omega_{cg}}{\omega_h} - \arctan\frac{\omega_{cg}}{\omega_b}} \tag{37}$$

with $\nu^* \in [1, 2]$ for CRONE-2.

D. Stability Analysis

Theorems 1 and 2 can be used to guarantee asymptotic stability using the following A_{cl}-matrix:

$$A_{cl} = \begin{bmatrix} \bar{A} & \bar{B}C_{nrp} \\ -B_{nrp}\bar{C} & A_{nrp} \end{bmatrix} \tag{38}$$

$$\nu^* = \frac{-\pi + M_\Phi - \angle G(j\omega_{cg}) + n_F \arctan\frac{\omega_{cg}}{\omega_F} + n_I\left(\frac{\pi}{2} - \arctan\frac{\omega_{cg}}{\omega_I}\right) - \Phi_r(\omega_{cg})}{\arctan\frac{\omega_{cg}}{\omega_h} - \arctan\frac{\omega_{cg}}{\omega_b}} \tag{36}$$

TABLE II
PARAMETERS OF CRONE-1 LAG RESET AND CRONE-2 LAG RESET CONTROLLERS

Symbol	Parameter	Value CRONE-1	Value CRONE-2
PM	phase margin	55°	55°
ω_{cg}	bandwidth	100 Hz	100 Hz
ω_b	lead corner frequency	12.5 Hz	12.5 Hz
ω_h	lag corner frequency	800 Hz	800 Hz
ω_I	integrator corner frequency	8.33 Hz	8.33 Hz
ω_F	low-pass filter corner frequency	1200 Hz	1200 Hz
n_I	integrator order	1	2
n_F	low-pass filter order	1	3
N	Oustaloup approximation order	4	4
p	reset percentage	0.5	0.5
γ	partial reset	0.5	0.5

where $(\bar{A}, \bar{B}, \bar{C}, \bar{D})$ are the state-space matrices of Σ_r^* and $(A_{nrp}, B_{nrp}, C_{nrp}, D_{nrp})$ are the state-space matrices of non-reset controller Σ_{nr} and plant Σ_p combined in series. $\bar{A}$ is defined as

$$\bar{A} = \begin{bmatrix} A_r & 0 \\ 0 & A_r \end{bmatrix} \tag{39}$$

$\bar{B}$ and $\bar{C}$ are defined, respectively, as

$$\bar{B} = \begin{bmatrix} B_r \\ B_r \end{bmatrix}, \quad \bar{C} = \begin{bmatrix} pC_r & (1-p)C_r \end{bmatrix} \tag{40}$$

and A_ρ^* is defined as

$$A_\rho^* = \text{diag}(\bar{A_\rho}, I_{n_r}, I_{n_{nrp}}) \tag{41}$$

where n_{nrp} is sum of the number of states of nonreset controller n_{nr} and plant n_p.

IV. PRACTICAL APPLICATION

The idea of CRONE reset control is to obtain a robust controller capable of overcoming the robustness-performance tradeoff. This is achieved by breaking Bode's gain-phase relation through introduction of nonlinearity. However, since the controller is analyzed and designed using the pseudolinear describing function approximation, the proposed controllers are tested on a precision positioning stage for validation.

A. System Overview

The system considered is a custom-designed one-degree-of-freedom nanometre precision positioning stage, actuated by a Lorentz actuator. This stage is linear-guided using flexures to attach the Lorentz actuator to the base of the stage and actuated at the center of the flexures. With a *Renishaw RLE10* laser encoder, the position of the stage is read out with 10 nm resolution. The setup is depicted in Fig. 6. All CRONE reset controllers are designed within a MATLAB/Simulink environment and implemented digitally via dSPACE DS1103 real-time control software with a sampling rate of 20 kHz. The transfer function of this system is identified as

$$P(s) = \frac{0.5474}{0.5718s^2 + 0.95 + 146.3} e^{-2.5 \times 10^{-4} s}. \tag{42}$$

The frequency response of the system is shown in Fig. 7 and shows the behavior of a second-order mass-spring-damper system with additional dynamics at higher frequencies and delay.

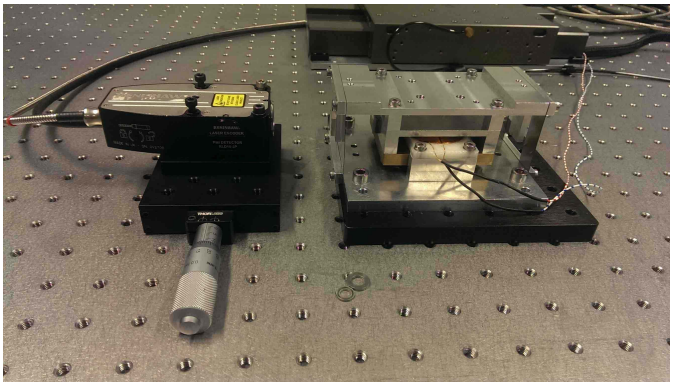

Fig. 6. Picture of the Lorentz stage (right) with the laser encoder (left).

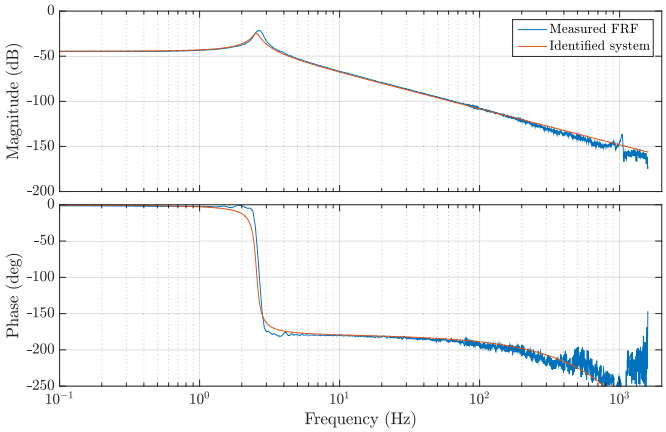

Fig. 7. Frequency response of the system and the identified system model.

B. Controller Design

The design of CRONE reset controllers for testing and validation provides us with choices over part of controller being reset as well as over the values of p and γ, resulting in infinite possible choices. In this paper, we have chosen resetting lag part and also $p = \gamma = 0.5$ for validation. Both CRONE-1 and CRONE-2 reset controllers are designed for the above-described positioning stage. The complete set of parameters of the two controllers can be found in Table II. Linear CRONE controllers are also designed with either $p = 1$ or $\gamma = 1$ or both, since all combinations result in linear CRONE design.

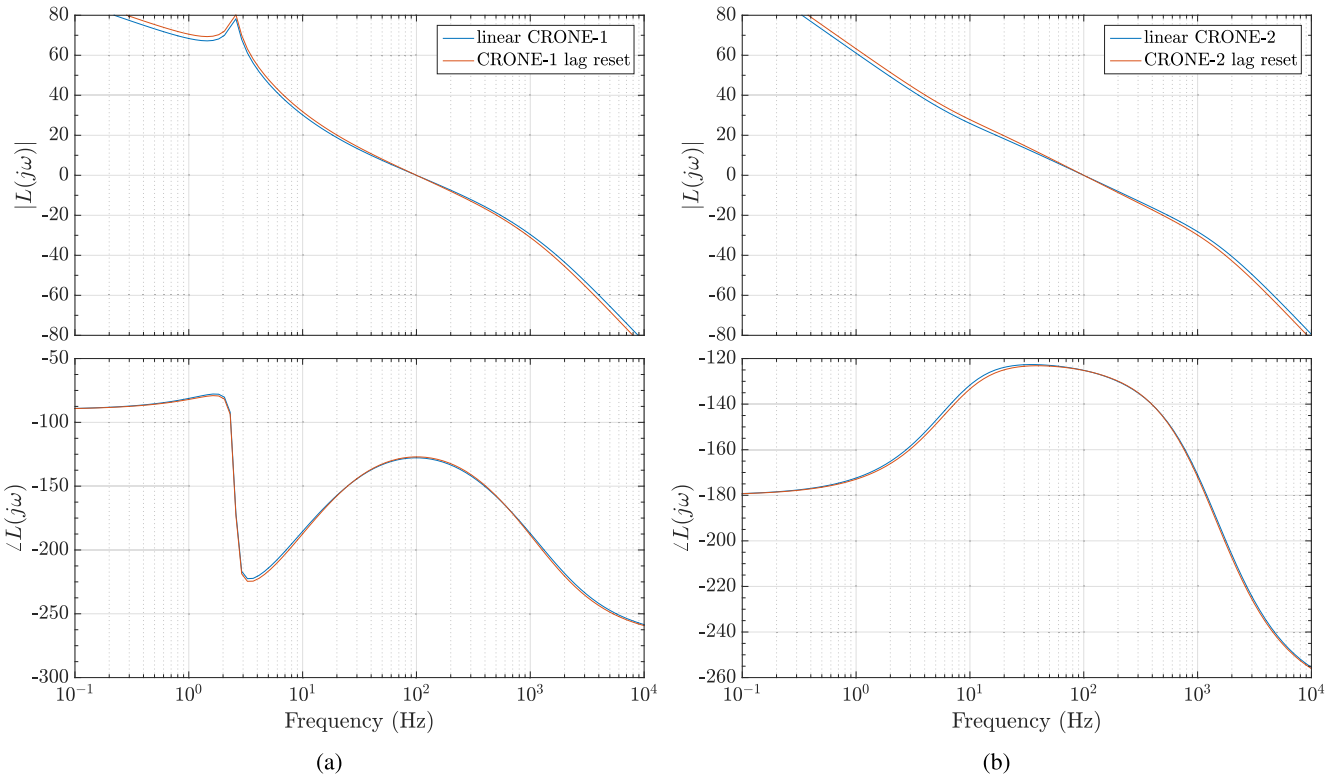

Fig. 8. Theoretical open-loop responses linear CRONE versus CRONE reset for (a) CRONE-1 lag reset and (b) CRONE-2 lag reset. The expected responses of CRONE reset are shown for $\gamma = p = 0.5$ as provided in Table. II

The theoretical open-loop responses are plot against its linear base equivalents in Fig. 8. Within these graphs, it is evident that for the same phase margin, the open-loop frequency response of CRONE reset provides a better open loop shape, i.e., higher gain at low frequency which should result in better tracking.

V. Experimental Results and Discussion

Experimental data have been retrieved for two purposes, namely: showing improvement in frequency domain through sensitivity functions and, thus, applicability of describing function analysis, and; showing improvement in time domain proving better robustness-performance tradeoffs of CRONE reset control compared to linear CRONE control.

A. Frequency-Domain Results

Complementary sensitivity function $T(j\omega)$ and sensitivity function $S(j\omega)$ were identified using a frequency sweep at the position of signal n in Fig. 9. $T(j\omega)$ then can be identified as the transfer from $-n$ to y, whereas $S(j\omega)$ is identified as the transfer from n to $y+n$. The frequency sweep was done from 0.1 Hz to 2.5 kHz with a target time of 120 s and a total duration of 480 s.

The identified frequency responses $S(j\omega)$ and $T(j\omega)$ for CRONE-1 lag reset and CRONE-2 lag reset for $\gamma = 0.5$ and different values of p are shown in Fig. 10. In the complementary sensitivity functions in Fig. 10(b) and (d), it can be seen that the peak value reduces for decreasing value

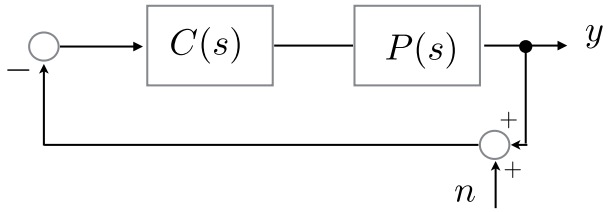

Fig. 9. Block diagram of the control loop and signals used for identification of $T(j\omega)$ and $S(j\omega)$.

of p (increasing nonlinearity in system). In addition, there is better attenuation of high frequencies. Both contribute to attaining better reference tracking performance.

In Fig. 10(a) and (c), the $S(j\omega)$ is shown for the same controller parameters. Here, it is evident that there is a gain reduction of both the peak value and sensitivity at higher frequencies. The low-frequency sensitivity functions are not shown for reasons of inevitable low coherence. The results presented above indicate an improvement in the robustness-performance tradeoff as decrease of both gain peak values and gain at low frequencies is observed.

B. Time-Domain Results: Reference Tracking

The fourth-order trajectory planning as in [32] is used to compute a triangular wave reference signal. This reference signal is representative of scanning motions in precision wafer stages. In addition, the second-order feedforward as formulated by the same authors has been implemented.

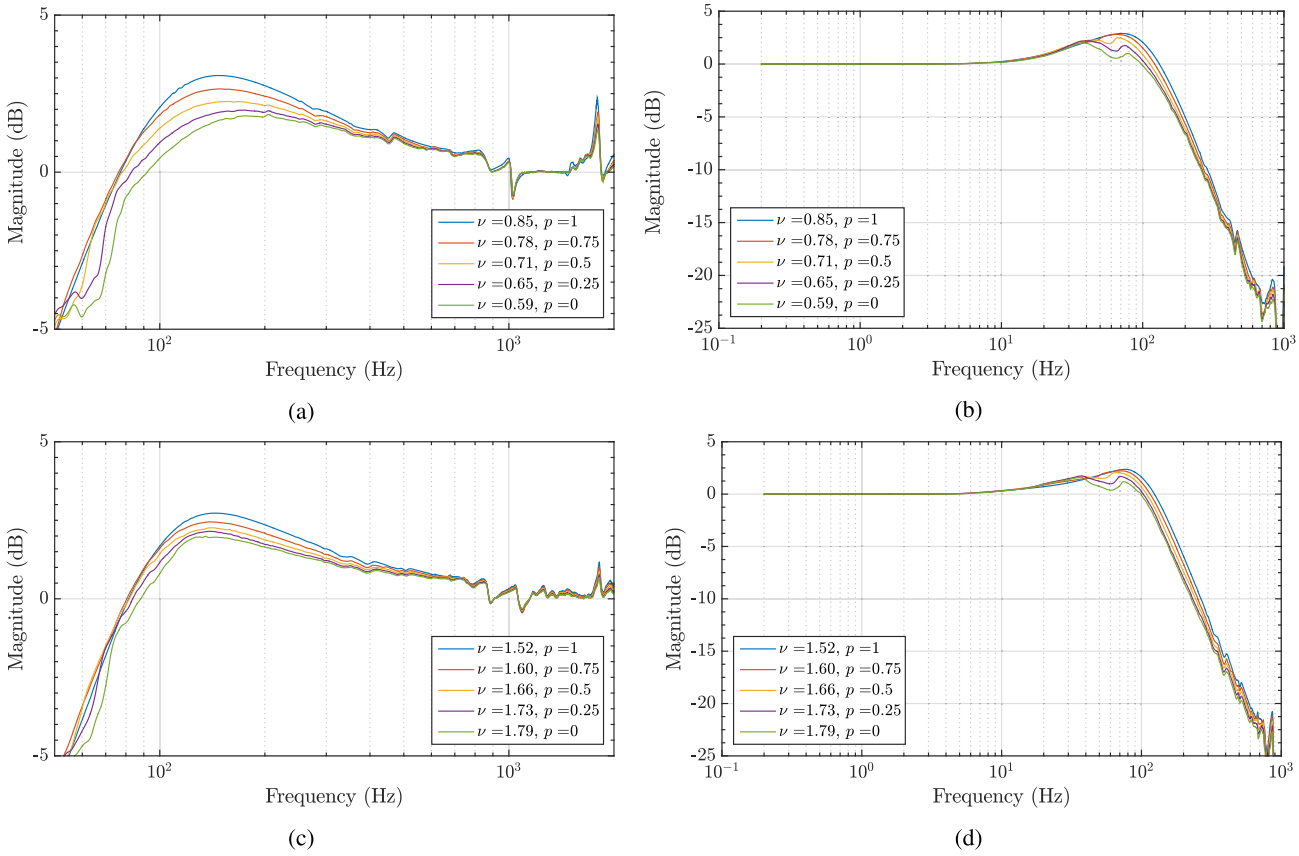

Fig. 10. Measured frequency responses for CRONE-1 lag reset (a) sensitivity function, (b) complementary sensitivity function and CRONE-2 lag reset, (c) sensitivity function, and (d) complementary sensitivity function for $\gamma = 0.5$ and different p-values.

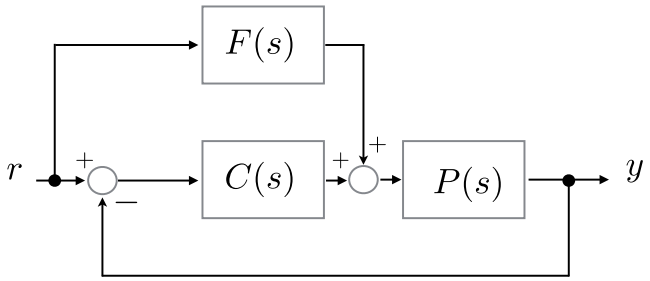

Fig. 11. Block diagram of the controlled system.

The feedforward controller provides a feedforward force F that is computed as

$$F = ma + cv \tag{43}$$

in which m is the stage mass, c is the damping coefficient, and a and v are the acceleration and velocity of the stage, respectively. In Fig. 11, a common feedforward controller $F(s)$ is used with linear CRONE and CRONE reset controllers as feedback controllers $C(s)$ for performance comparison.

The tracking errors for the CRONE lag reset controllers are compared to linear CRONE controllers for the same phase margin shown in Fig. 12. According to theory, as has been explained in Section III, the CRONE reset system will perform better than the linear CRONE reset system with similar phase margin. This is confirmed by the measurements and is evident from the error plots shown in Fig. 12. For CRONE-1 lag reset, the rms error reduces from 22.1 to 19.6 nm compared to the linear CRONE-1 controller. For CRONE-2 lag reset, rms error is reduced from 70.7 to 52.8 nm. Hence, better performance in terms of reference tracking has been achieved in CRONE reset control compared to linear CRONE. This improvement in tracking performance is also in line with the $S(j\omega)$ graphs shown in Fig. 10(a) and (c), which is basically an estimate of the error with respect to reference.

It has to be noted that the maximum control effort peaks are larger in the nonlinear system. Nevertheless, if the system does not suffer from control saturation, this increase is no problem.

C. Time-Domain Results: Noise Attenuation

The noise-attenuation performance of the CRONE lag reset and linear CRONE reset controllers is evaluated using the system response to a sine noise input signal. Noise power is calculated for sine signal of different frequencies above the bandwidth for a duration of 5s. The decrease in average power in decibels for $p = \gamma = 0.5$ with respect to linear case is shown in Tables III and IV. In the literature, one of the most noted advantages of reset is its improved performance in noise attenuation. This property of reset is validated again in the case of CRONE reset with these results. These results provide further validation of $T(j\omega)$ plotted in Fig. 10(b) and (d), which is an estimate of error due to the noise at a range of frequencies.

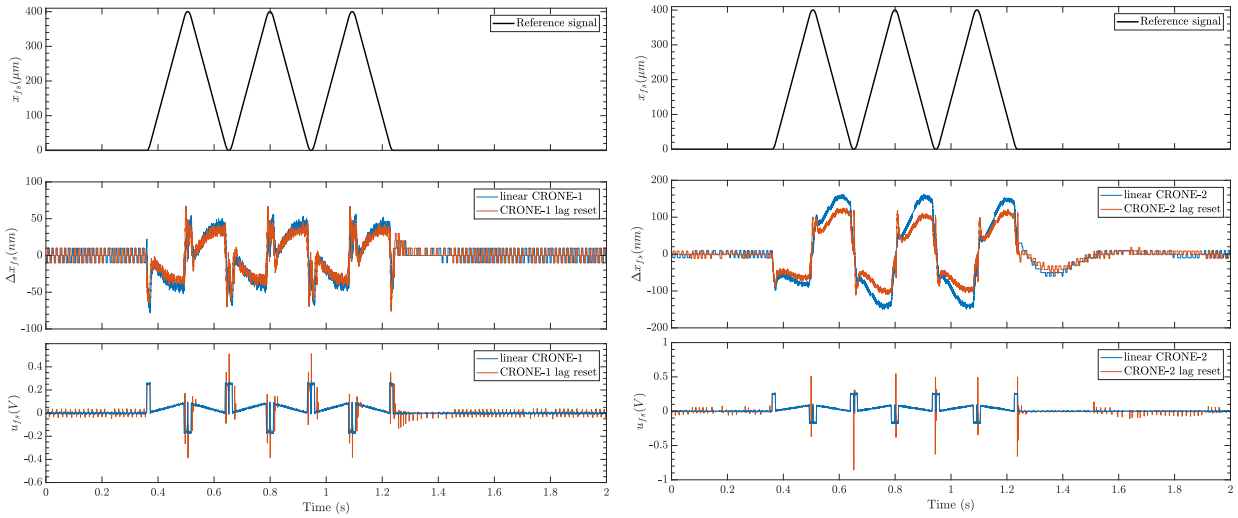

Fig. 12. Reference tracking of a fourth-order input-shaped triangular wave signal for (a) CRONE-1 lag reset and (b) CRONE-2 lag reset compared to linear CRONE for the same phase margin.

TABLE III

REDUCTION OF AVERAGE POWER OF NOISE RESPONSE FOR $\gamma = 0.5$, $p = 0.5$ WITH RESPECT TO LINEAR CASE FOR CRONE-1

Frequency (Hz)	noise reduction (dB)
300	2.46
400	2.74
500	2.72
600	2.98
700	2.66
800	2.57
900	1.79
1000	2.59

TABLE IV

REDUCTION OF AVERAGE POWER OF NOISE RESPONSE FOR $\gamma = 0.5$, $p = 0.5$ WITH RESPECT TO LINEAR CASE FOR CRONE-2

Frequency (Hz)	noise reduction (dB)
300	2.94
400	3.14
500	3.55
600	3.14
700	3.30
800	3.10
900	3.93
1000	2.92

D. Time-Domain Results: Disturbance Rejection

A large percentage of the high precision achieved in the high-tech industry is due to the accurate design of the feedforward controller. In several cases, the feedforward controller and the reference itself are designed so well that the feedback controller does not see any error due to the change in reference. In such a scenario, the feedback controller is mainly responsible for noise attenuation and disturbance rejection. The improved noise attenuation performance of CRONE reset controllers has already been validated in the previous section.

TABLE V

SETTLING TIME (TIME TO REACH 15% OF PEAK VALUE $\hat{x}_{fs}$) FOR CRONE-1 RESET CONTROLLERS WITH VALUE OF γ FIXED TO 0.5

p	$\hat{x}_{fs}$ ()nm)	settling time (ms)
1	530	55.8
0.75	540	65.5
0.5	540	65.5
0.25	550	66.0
0	560	76.8

TABLE VI

SETTLING TIME (TIME TO REACH 15% OF PEAK VALUE $\hat{x}_{fs}$) FOR CRONE-2 RESET CONTROLLERS WITH VALUE OF γ FIXED TO 0.5

p	$\hat{x}_{fs}$ ()nm)	settling time (ms)
1	570	146.0
0.75	570	135.7
0.5	570	128.1
0.25	590	125.1
0	600	68.3

The response of CRONE reset controllers for a step disturbance is shown in Fig. 13. While the maximum error due to this disturbance is not significantly different in the responses of CRONE reset and linear CRONE, significant difference is seen in the settling time. The settling time is defined and calculated as the time required to decrease to 15% of the maximum peak value. The computed settling times are given in Tables V and VI for CRONE-1 reset and CRONE-2 reset, respectively.

In the case of disturbance rejection, it is seen that the performance of the controllers does not match the expectation from describing function. While in the case of CRONE-2 reset controllers, a reduction in settling time is seen, there is a slight increase in maximum displacement due to disturbance.

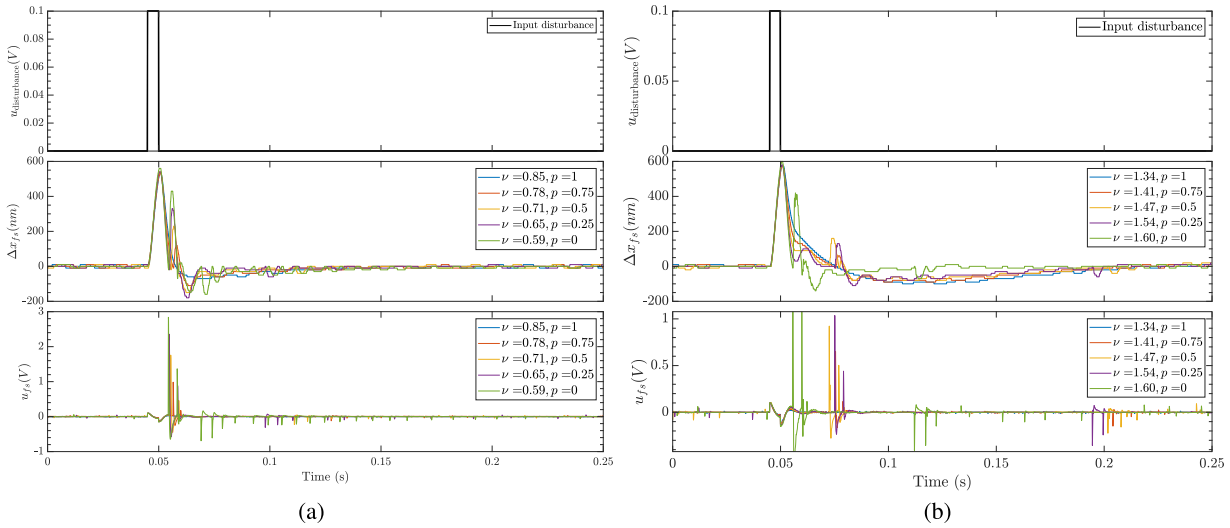

Fig. 13. Response to a pulse disturbance for lag reset with $\gamma = 0.5$ for (a) CRONE-1 lag reset and (b) CRONE-2 lag reset.

However, in the case of CRONE-1, significant rise in settling time is also seen. This could possibly be explained as effect of higher order harmonics introduced by reset. These results also show that while describing functions are reliable in estimating performance improvement in some cases, they are not reliable under all circumstances. This discrepancy is even more evident when we consider that process sensitivity which is the estimate of error with respect to disturbance can be obtained in linear systems by multiplying sensitivity with the plant being controlled. The sensitivity $S(j\gamma)$ for the designed controllers is plotted in Fig. 10(b) and (d). Since the plant is constant for all the designed controllers, the disturbance rejection performance should follow the describing function estimation. However, this is not the case as seen from the practical results. Hence, new frequency-domain tools capable of accurately estimating closed-loop performance of reset systems are required.

VI. Conclusion

The first part of this paper has a theoretical focus: novel and general design rules are developed in the synthesis of the proposed CRONE reset controller. These general rules are applicable to a broad range of reset strategies that can be taken for both first generation CRONE reset and second generation CRONE reset. The developed theory was used in the design of a CRONE-1 lag reset and CRONE-2 lag reset controller. For these controllers, it was shown that for similar phase margin, better open-loop shape can be achieved compared to linear CRONE control, thus providing relief from Bode's fundamental gain-phase relation and fundamental robustness-performance tradeoffs.

In the second part of this paper, the designed CRONE reset controllers have been validated on a Lorentz-actuated precision stage. First, it was shown that the sensitivity function and complementary sensitivity function, which were identified from the measurement data, improve in the frequency range of interest. Both sensitivity and complementary sensitivity peaks reduced as well as gain at high frequencies. Using time-domain reference-tracking results for a fourth-order input-shaped triangular reference signal, it was shown that the better open-loop shape of CRONE-reset, indeed, improves reference-tracking performance. For both CRONE-1 lag reset and CRONE-2 lag reset, reduction in rms tracking error was observed. The use of reset for improved noise rejection performance is also validated on the practical setup.

The reliability of describing function, however, is questionable in the case of disturbance rejection. While in the case of CRONE-2, reset improvement is seen in settling time, performance deteriorates both in terms of maximum displacement and settling time for CRONE-1 reset.

Several challenges of reset control are not addressed in this paper but will be considered in future work. These include limit cycles, low-frequency disturbances, and higher order harmonic behavior amongst others. As seen with the results of disturbance rejection, existing analysis of open-loop and closed-loop behavior of reset systems using describing function is insufficient under certain conditions. This requires new tools and methodologies for frequency-domain analysis of reset systems. However, the results shown in this paper are already promising: for the designed CRONE reset controllers with partial reset and reset percentage already improve tracking performance and noise attenuation with respect to linear CRONE. This means that with the future study into the effect of higher order harmonics, performance of CRONE reset can be further improved. Also, such a study of higher order harmonics will provide more insight into the choice of values of p and γ. While 0.5 has been chosen as the value for comparison and validation in this paper, the best value to achieve required specifications for any system can be accurately chosen when the complete closed-loop performance including the effect of higher order harmonics can be predicted.

References

[1] S. Skogestad and I. Postlethwaite, *Multivariable Feedback Control: Analysis and Design*. New York, NY, USA: Wiley, 2007.

[2] R. M. Schmidt, G. Schitter, and A. Rankers, *The Design of High Performance Mechatronics: High-Tech Functionality by Multidisciplinary System Integration*, 2nd ed. Amsterdam, The Netherlands: IOS Press, 2014.

[3] K. K. Tan, T. H. Lee, and S. Huang, *Precision Motion Control: Design and Implementation*. Berlin, Germany: Springer, 2007.

[4] J. Sabatier, P. Lanusse, P. Melchior, and A. Oustaloup, *Fractional Order Differentiation and Robust Control Design: CRONE, H-Infinity and Motion Control*. Berlin, Germany: Springer, vol. 10, 2015.

[5] J. Clegg, "A nonlinear integrator for servomechanisms," *Trans. Amer. Inst. Electr. Eng. II, Appl. Ind.*, vol. 77, no. 1, pp. 41–42, Mar. 1958.

[6] M. Vidyasagar, in *Nonlinear systems Analysis*. Philadelphia, PA, USA: Siam, vol. 42, 2002.

[7] C. Prieur, S. Tarbouriech, and L. Zaccarian, "Improving the performance of linear systems by adding a hybrid loop," *IFAC Proc. Vols.*, vol. 44, no. 1, pp. 6301–6306, Jan. 2011. [Online]. Available: http://www.sciencedirect.com/science/article/pii/S147466701644615X

[8] G. Witvoet, W. H. T. M. Aangenent, W. P. M. H. Heemels, M. J. G. van de Molengraft, and M. Steinbuch, "H2 performance analysis of reset control systems," in *Proc. 46th IEEE Conf. Decision Control*, Dec. 2007, pp. 3278–3284.

[9] J. Zheng, Y. Guo, M. Fu, Y. Wang, and L. Xie, "Development of an extended reset controller and its experimental demonstration," *IET Control Theory Appl.*, vol. 2, no. 10, pp. 866–874, Oct. 2008.

[10] A. Baños, S. Dormido, and A. Barreiro, "Stability Analysis of reset control systems with reset band," *IFAC Proc. Vols.*, vol. 42, no. 17, pp. 180–185, 2009.

[11] A. Vidal and A. Baños, "Reset compensation for temperature control: Experimental application on heat exchangers," *Chem. Eng. J.*, vol. 159, nos. 1–3, pp. 170–181, May 2010. [Online]. Available: http://www.sciencedirect.com/science/article/pii/S1385894710001452

[12] A. Vidal, A. Banos, J. C. Moreno, and M. Berenguel, "PI+CI compensation with variable reset: Application on solar collector fields," in *Proc. IEEE Annu. Conf. Ind. Electron.*, Nov. 2008, pp. 321–326.

[13] A. Baños and A. Vidal, "Definition and tuning of a PI+CI reset controller," in *Proc. Eur. Control Conf. (ECC)*. Jul. 2007, pp. 4792–4798.

[14] A. Ba nos, J. Carrasco, and A. Barreiro, "Reset times-dependent stability of reset control systems," *IEEE Trans. Autom. Control*, vol. 56, no. 1, pp. 217–223, Jan. 2011.

[15] S. J. L. M. Van Loon, K. G. J. Gruntjens, M. F. Heertjes, N. Van de Wouw, and W. P. M. H. Heemels, "Frequency-domain tools for stability analysis of reset control systems," *Automatica*, vol. 82, pp. 101–108, Aug. 2017.

[16] H. Li, C. Du, and Y. Wang, "Optimal reset control for a dual-stage actuator system in HDDs," *IEEE/ASME Trans. Mechatronics*, vol. 16, no. 3, pp. 480–488, Jun. 2011.

[17] J. Carrasco, A. Baños, and A. van der Schaft, "A passivity-based approach to reset control systems stability," *Syst. Control Lett.*, vol. 59, no. 1, pp. 18–24, Jan. 2010. [Online]. Available: http://www.sciencedirect.com/science/article/pii/S0167691109001352

[18] A. Baños and A. Barreiro, *Reset Control Systems*. Berlin, Germany: Springer, 2011.

[19] M. A. Davó and A. Baños, "Reset control of a liquid level process," in *Proc. IEEE 18th Conf. Emerg. technol. Factory Autom. (ETFA)*, Sep. 2013, pp. 1–4.

[20] F. Perez, A. Baños, and J. Cervera, "Periodic reset control of an in-line pH process," in *Proc. ETFA*, Sep. 2011, pp. 1–4.

[21] L. Hazeleger, M. Heertjes, and H. Nijmeijer, "Second-order reset elements for stage control design," in *Proc. Amer. Control Conf. (ACC)*, Jul. 2016, pp. 2643–2648.

[22] Y. Li, G. Guo, and Y. Wang, "Reset control for midfrequency narrowband disturbance rejection with an application in hard disk drives," *IEEE Trans. Control Syst. Technol.*, vol. 19, no. 6, pp. 1339–1348, Nov. 2011.

[23] H. Li, C. Du, and Y. Wang, "Discrete-time H_2 optimal reset control with application to HDD track-following," in *Proc. Chin. Control Decision Conf.*, Jun. 2009, pp. 3613–3617.

[24] S. H. HosseinNia, I. Tejado, and B. M. Vinagre, "Basic properties and stability of fractional-order reset control systems," in *Proc. IEEE Eur. Control Conf. (ECC)*, Jul. 2013, pp. 1687–1692.

[25] S. H. HosseinNia, I. Tejado, D. Torres, B. M. Vinagre, and V. Feliu, "A general form for reset control including fractional order dynamics," *IFAC Proc. Vols.*, vol. 47, no. 3, pp. 2028–2033, 2014.

[26] N. Saikumar and S. H. Hosseinnia, "Generalized fractional order reset element (GFrORE)," in *Proc. 9th Eur. Nonlinear Dyn. Conf. (ENOC)*, Jun. 2017.

[27] S. H. HosseinNia, I. Tejado, B. M. Vinagre, and Y. Chen, "Iterative learning and fractional reset control," in *Proc. ASME Int. Design Eng. Tech. Conf. Comput. Inf. Eng. Conf.*, vol. 9, Aug. 2015, pp. 1–8. [Online]. Available: https://doi.org/10.1115/detc2015-47061

[28] L. Chen, N. Saikumar, S. Baldi, and S. H. HosseinNia, "Beyond the waterbed effect: Development of fractional order CRONE control with non-linear reset," in *Proc. Annu. Amer. Control Conf. (ACC)*, Jun. 2018, pp. 545–552.

[29] Y. Guo, Y. Wang, and L. Xie, "Frequency-domain properties of reset systems with application in hard-disk-drive systems," *IEEE Trans. Control Syst. Technol.*, vol. 17, no. 6, pp. 1446–1453, Nov. 2009.

[30] O. Beker, C. Hollot, Y. Chait, and H. Han, "Fundamental properties of reset control systems," *Automatica*, vol. 40, no. 6, pp. 905–915, Jun. 2004.

[31] D. Nešić, L. Zaccarian, and A. R. Teel, "Stability properties of reset systems," *Automatica*, vol. 44, no. 8, pp. 2019–2026, Aug. 2008.

[32] P. Lambrechts, M. Boerlage, and M. Steinbuch, "Trajectory planning and feedforward design for electromechanical motion systems," *Control Eng. Pract.*, vol. 13, no. 2, pp. 145–157, Feb. 2005. [Online]. Available: http://www.sciencedirect.com/science/article/pii/S0967066104000462

Linda Chen received the B.Sc. degree in applied physics and the M.Sc. degree in systems and control from the Delft University of Technology, Delft, The Netherlands, in 2015 and 2017, respectively. Her master thesis was on the Development of CRONE Reset Controlâ and was performed in the collaboration between the Delft Center for Systems and Control and the Department of Precision and Microsystems Engineering, Delft University of Technology.

Niranjan Saikumar received the Ph.D. degree in electrical engineering specializing in learning control for mechatronic applications from the Indian Institute of Science, Bangalore, India, in 2016.

Since 2016, he has been holing a postdoctoral position with the Department of Precision and Microsystems Engineering, TU Delft, Delft, the Netherlands. His current research interests include mechatronic system design, precision motion control, and nonlinear and learning control methods.

S. Hassan HosseinNia (SM'18) received the Ph.D. degree *(summa cum laude)* in electrical engineering specializing in automatic control: application in mechatronics from the University of Extremadura, Badajoz, Spain, in 2013.

He has an industrial background with ABB, Västerås, Sweden. Since 2014, he has been an Assistant Professor with the Department of Precision and Microsystems Engineering, TU Delft, Delft, the Netherlands. His current research interests include precision mechatronic system design, precision motion control, and mechatronic system with distributed actuation and sensing.

Dr. HosseinNia has been an Associate Editor of the *International Journal of Advanced Robotic Systems* since 2017.